JACS
JOURNAL OF THE AMERICAN CHEMICAL SOCIETY
Communication
pubs.acs.org/JACS

Synthesis of Convex Hexoctahedral Pt Micro/Nanocrystals with High-Index Facets and Electrochemistry-Mediated Shape Evolution

Jing Xiao, Shuo Liu, Na Tian,* Zhi-You Zhou, Hai-Xia Liu, Bin-Bin Xu, and Shi-Gang Sun*

State Key Laboratory of Physical Chemistry of Solid Surfaces, Department of Chemistry, College of Chemistry and Chemical Engineering, Xiamen University, Xiamen 361005, China

Supporting Information

ABSTRACT: Systematic manipulation of nanocrystal shapes is prerequisite for revealing their shape-dependent physical and chemical properties. Here we successfully prepared a complex shape of Pt micro/nanocrystals: convex hexoctahedron (HOH) enclosed with 48 {15 5 3} high-index facets by electrochemical square-wave-potential (SWP) method. This shape is the last crystal single form that had not been achieved previously for face-centered-cubic (fcc) metals. We further realized the shape evolution of Pt nanocrystals with high-index facets from tetrahexahedron (THH) to the HOH, and finally to trapezohedron (TPH) by increasing either the upper (E_U) or lower potential (E_L). The shape evolution, accompanied by the decrease of low-coordinated kink atoms, can be correlated with the competitive interactions between preferentially oxidative dissolution of kink atoms at high E_U and the redeposition of Pt atoms at the E_L.

Perfect nanocrystals exhibit a variety of highly symmetric polyhedral shapes and have fascinated artists and scientists.[1] Better understanding of nanocrystal growth habits and systematic controlling of their shapes/surface structures are very important for uncovering many shape-dependent physical and chemical properties, especially catalytic performance.[2] As for face-centered-cubic (fcc) metals, single-crystal nanocrystals enclosed by uniform facets (termed as simple forms) have seven typical shapes: cube, octahedron, rhombic dodecahedron (RD), tetrahexahedron (THH), trapezohedron (TPH), trisoctahedron (TOH), and hexoctahedron (HOH), and their exposed facets are {100}, {111}, {110}, {*hk*0}, {*hkk*}, {*hhl*}, and {*hkl*}, where $h > k > l \geq 1$, respectively, as shown in Figure 1.[3]

The nanocrystals enclosed by {100} and {111} facets can be synthesized easily because of low surface energy and have been well documented in literature.[2a,4] Other complex-shaped nanocrystals have high surface energy, mainly originated from low-coordinated step or kink atoms. The synthesis of these high-energy nanocrystals is quite difficult, as the growth rate along a facet increases exponentially with increasing its surface energy, and fast-growing facets will disappear spontaneously because of the law of constancy of interfacial angle.[5] Nevertheless, considerable progress has still been made in this filed in recent years,[6] especially stimulated by electrochemical synthesis of Pt THH.[7] So far, a variety of Pt, Pd, and Au nanocrystals with high-index facets, including THH,[8] TPH,[3a,9] TOH,[10] and even concave HOH shapes,[3a,11] have been synthesized. There is just one single form missing: convex HOH. As shown in Figure 1, convex HOH represents the most complex crystal form of fcc metals, and it is enclosed by a total of 48 {*hkl*} high-index facets. These facets contain kink atoms with a very low coordination number (CN) of six. More uniquely, the {*hkl*} facets have chirality, and nanocrystals with {*hkl*} facets can be used as chiral catalysts.[12]

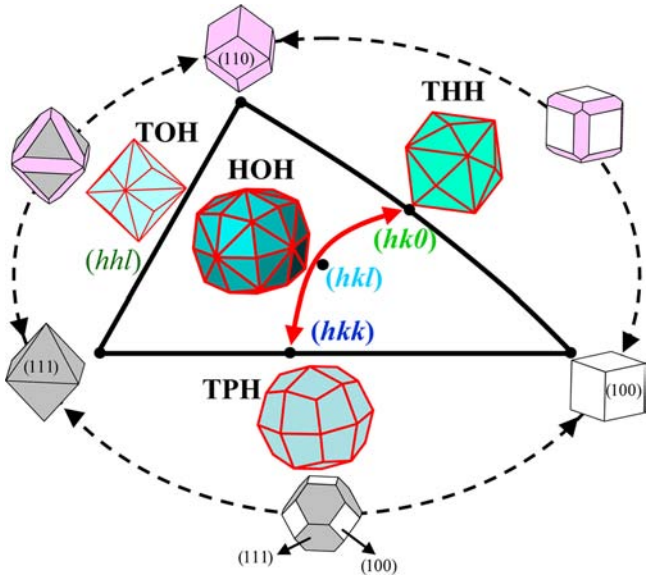

Figure 1. Illustration of shape evolution of fcc metal nanocrystals enclosed by different facets in unit stereographic triangle. Low-index faceted (i.e., (111), (100), and (110)) nanocrystal evolution occurs via truncated shapes. High-index faceted nanocrystal evolution occurs via gradual changing of surface structures/Miller indices.

The study of nanocrystal shape evolution is also a hot topic in nanomaterial field, as it is vital for systematic manipulation of nanocrystal surface structures. As for nanocrystals with low-index facets (i.e., {100}, {111}, and {110}), the shape evolution among them is observed through a series of truncated shapes (such as cuboctahedron) to change the relative proportions of exposed facets,[4,13] as illustrated in Figure 1. For example, Xu and co-workers have reported a seed-mediated method for systematic control of polyhedral Pd nanocrystals among cube, octahedron, rhombic dodecahedron, as well as all kinds of

Received: October 16, 2013
Published: December 3, 2013

dx.doi.org/10.1021/ja410583b | J. Am. Chem. Soc. 2013, 135, 18754−18757

truncated shapes.[13b] Xia's group found that the combining oxidative etching with regrowth can induce the shape transformation among low-index-faceted Pd nanocrystals.[13c] However, to the best of our knowledge, there is no report so far involving shape evolution among high-index faceted nanocrystals, which is critical for understanding their formation mechanism, so as to rationally engineer nanocrystals with desirable surface structures and exceptional properties.

Herein, we report the successful synthesis of convex HOH Pt nanocrystals for the first time by an electrochemical square-wave-potential (SWP) method. Furthermore, we observed that Pt HOH can serve as a bridge to shape evolution of Pt nanocrystals from THH to TPH or vice versa. A possible mechanism is proposed for electrochemically mediated shape evolution of Pt nanocrystals with high-index facets.

High-index faceted Pt nanocrystals were electrodeposited on a glassy carbon (GC, ϕ = 6 mm) electrode in 2 mM H_2PtCl_6 + 0.1 M H_2SO_4 solution. In brief, the GC electrode was first subjected to a potential step from 1.20 to −0.30 V (versus saturated calomel electrode (SCE) scale), and held for 140 ms to generate crystal nuclei. The growth of the nuclei to Pt nanocrystals was then achieved by the SWP (f = 100 Hz) for 20 min. The shapes of Pt nanocrystals could be tuned through changing either lower (E_L) or upper (E_U) potential limit. The morphology and structure of the Pt nanocrystals were characterized by scanning electron microscopy (SEM, Hitachi S-4800) and transmission electron microscopy (TEM, JEM-2100 at 200 kV).

Figure 2 shows low- and high-magnification SEM images of Pt nanocrystals prepared at E_L = 0.12 V and E_U = 1.05 V,

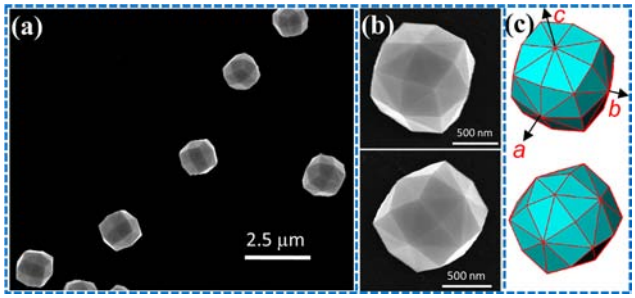

Figure 2. (a) Low- and (b) high-magnification SEM images of convex HOH Pt nanocrystals. (c) Corresponding HOH models oriented at the same directions as nanocrystals in (b).

manifesting the predominance and uniformity of convex HOH Pt nanocrystals. The shape of convex HOH can be seen as an octahedron by dividing each of the octahedron's eight faces into six triangular faces, as shown in Figure 2c (six faces among a, b, and c axes). The nanocrystals (Figure 2b) match well with the HOH models (Figure 2c) projected at the same orientations, confirming the successful synthesis of convex Pt HOH. The yield of Pt HOH is over 90%. The size distribution of Pt HOH is rather broad, ranging from 350 nm to 1.6 μm with an average value of 1.03 μm (Figure S1, Supporting Information (SI)). Therefore, it is difficult to control the uniformity of particle size currently. As the particle size depends on the growth time, the Pt nanocrystals obtained in the early stage (1 min) seem like HOH shape, and have a particle size ranging from 30 to 70 nm (Figure S2 (SI)). Note that although there are a few reports about the HOH metal nanocrystals synthesized by both wet-chemical and electrochemical methods, all of them are concave shape.[3a,11] The concave shape is relatively easy to achieve because of the fast mass transfer at the corners/tips.

We used TEM to determine surface structure of the Pt HOH. Since convex HOH shape is very complex and the three Miller indices (h, k, and l) are different, it is more difficult to indentify them as compared with other shapes such as THH.[7] We measured TEM images of the Pt HOH along [111], [110], and [100] directions (Figure 3a−c), as evidenced by

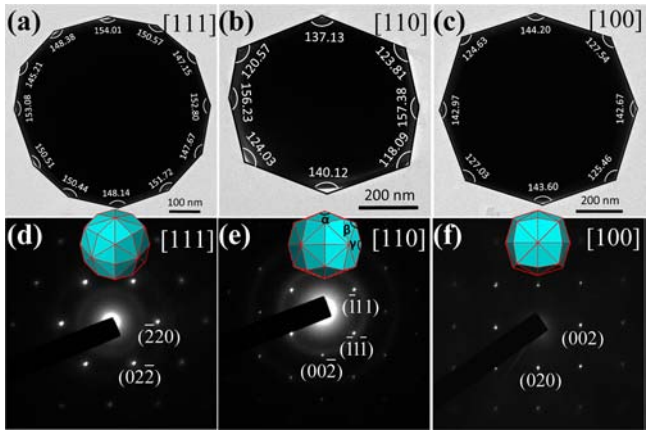

Figure 3. TEM images (a−c) and corresponding SAED patterns (d−f) of Pt HOH along the [111], [110], and [100] directions. Insets are corresponding HOH models oriented at the same directions.

corresponding selected-area electron diffraction (SAED) patterns (Figure 3d−f). The ideal projections of HOH model along above three directions are dodecagon, octagon, and octagon (insets to Figure 3), in good agreement with the outline of TEM images of the Pt nanocrystals. This result further confirms the successful synthesis of convex Pt HOH. We further deduced the general expressions of projection angles of fcc metal nanocrystals as a function of Miller indices (Figure S3 (SI)). We found that the surface structure of HOH nanocrystals can be best revealed by measuring the projection along [110] crystal axis, where three projection angles (α, β, and γ) are associated with three Miller indices. In the TEM image (Figure 3b), the average value of α, β, and γ are 138.6°, 121.6°, and 156.8°, respectively, very close to the theoretical values (138.67°, 122.64°, and 156.05°) for HOH model with {15 5 3} facets. Moreover, the projection angles of Pt HOH along [111] and [100] directions also coincide well with those of HOH models with {15 5 3} facets (Table S1 (SI)). So, the as-prepared Pt HOH nanocrystals are mainly bounded by {15 5 3} high-index facets.

We further found that the Pt HOH can serve as a bridge to shape evolution from THH to TPH, two types nanocrystals with {$hk0$} and {hkk} high-index facets, respectively. As illustrated in Figure 4, the shapes of Pt nanocrystals can be easily tuned by the change of either the E_L or E_U. More SEM and TEM images of these Pt nanocrystals are shown in Figures S4−S12 (SI). Pt THH could be obtained at E_L = 0.12 V and E_U = 1.00 V. The surface structure of the Pt THH was identified as mainly {730} facets (Figure S4 and Table S2 (SI)). Slightly increasing the E_U to 1.02 V, the shape of Pt nanocrystals changed to imperfect HOH, whose surface is not smooth with many light scratches (see high-magnification SEM image in Figure S5 (SI)). Further increasing the E_U to 1.05 V, the perfect Pt HOH with {15 5 3} facets could be obtained (Figure 2). When the E_U was increased to 1.07 V, the HOH shape

dx.doi.org/10.1021/ja410583b | J. Am. Chem. Soc. 2013, 135, 18754−18757

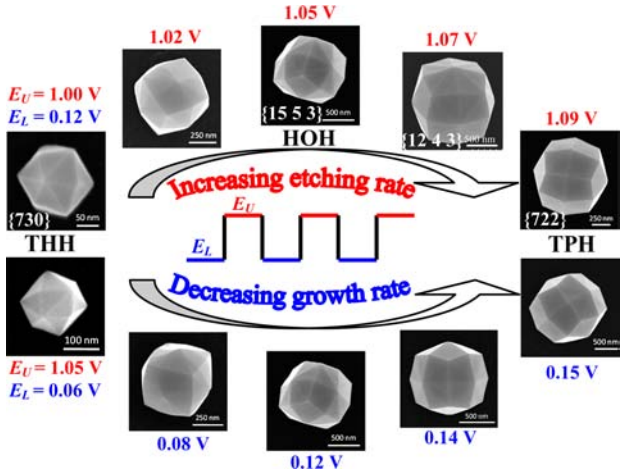

Figure 4. Shape evolution of Pt nanocrystals from THH to TPH via HOH by increasing the E_U or E_L of the SWP. Increasing E_U will increase the etching rate, and increasing E_L will decrease growth rate of Pt nanocrystals. Both approaches result in the same trend of shape evolution.

gradually changed to TPH shape. The Miller indices of exposed surface was identified as {12 4 3} facets (Figures S6 and S7 and Table S3 (SI)), very close to {311} facets on TPH. Further increasing the E_U to 1.09 V, perfect TPH nanocrystals with {722} facets (Figure S8 (SI)) were obtained. Similar trend of shape evolution can also be achieved by fixing the E_U at 1.05 V, while gradually increasing the E_L from 0.06 to 0.15 V.

Clearly, the behavior of shape evolution for high-index faceted nanocrystals observed here is significantly different from that for low-index faceted nanocrystals. In the latter case, shape evolution is realized through the truncated forms (such as cuboctahedron enclosed by the mixture of (111) and (100) facets) to change the relative proportions of exposed facets. For high-index facets, their {*hkl*} Miller indices are variable, so the shape evolution can occur through gradually changing Miller indices or surface structure while keeping homogeneous facets. The difference between two types of shape evolution can be seen clearly in Figure 1.

Figure 5a–d demonstrates the corresponding evolution of surface structures of Pt nanocrystals mediated by changing the E_U. Pt(730) surface is periodically composed of two (210) subfacets followed by one (310) subfacet.[7] This surface essentially consists of (100) as terrace and (110) as step. The (110) step can be further divided into monatomic width of (111) and monatomic width of (11$\bar{1}$), as shown in Figure 5a. This surface has kink atoms (marked by "●") with a CN of 6 but has no chiral feature. As the E_U increases, the surface changes to more complex Pt(15 5 3). As illustrated in Figure 5b, the (15 5 3) is still with (100) as terrace, but the step becomes asymmetric zigzag structure with four atomic width of (111) and monatomic width of (11$\bar{1}$). As a consequence, this type of kink site has chirality. Another feature is that the density of kink atoms decreases greatly from 5.12×10^{14} cm^{-2} on (730) facet to 1.61×10^{14} cm^{-2} on (15 5 3) facet, 1.00×10^{14} cm^{-2} on (12 4 3) facet, and essentially zero on (722) facet. However, the sum of step and kink atoms only changes slightly for these four surfaces (Table S4 (SI)).

The evolution of Pt nanocrystal shapes and corresponding surface structures may be correlated with multiple effects of the SWP, as illustrated in Figure 5e. At the E_U, oxygen species (OH_{ad} and O_{ad}), originating from H_2O dissociation, will adsorb

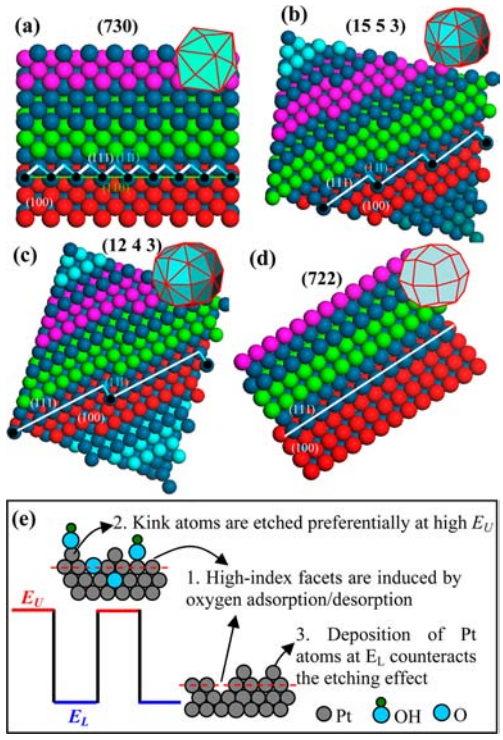

Figure 5. Atomic models of Pt high-index facets obtained by increasing E_U. (a) (730) at E_U = 1.00 V; (b) (15 5 3) at E_U = 1.05 V; (c) (12 4 3) at E_U = 1.07 V; (d) (722) at E_U = 1.09 V. Kink atoms are marked by "●". Clearly, the amount of kink atoms decreases with increasing E_U. (e) Illustration of multiple effects of SWP on the surface structures of Pt nanocrystals.

on the Pt surfaces, and some of them may invade into Pt surface through place-exchange between Pt atoms and oxygen atoms.[14] As a result, some Pt atoms are squeezed out. At the E_L, all oxygen species will be reductively desorbed. However, the displaced Pt atoms cannot always return to their original positions, leading to the formation of step or kink sites. The above oxygen adsorption/desorption are repeated thousands of times under the SWP conditions, and well-defined high-index facets will form finally (Process 1 in Figure 5e).[7,14] The oxygen adsorption can also decrease greatly surface energy of Pt and stabilize the high-index facets. The importance of oxygen adsorption can be verified by the following control experiment: if the E_U is too low (e.g., 0.90 V) to generate intensive oxygen adsorption, Pt high-index facets cannot form (Figure S13 (SI)).

One question arises why kink atoms decrease along with increasing the E_U or E_L. This may be attributed to other effects of SWP. If the E_U is high enough (e.g., > 1.0 V), some kink atoms can be preferentially etched out because of low CN in comparison with step and terrace atoms (Process 2). The preferential etching of kink atoms on Pt surface has been observed by in situ STM studies.[15] Clearly, the etching rate will increase with increasing E_U, resulting in the decrease of the number of kink atoms. In contrast, at the E_L, new Pt atoms will be deposited on the surface through the reduction of $PtCl_6^{2-}$ in solution (Process 3). If the Pt atoms are deposited at step sites, new kink sites may be created. Obviously, the regrowth process at the E_L will counteract the etching effect at the E_U: the lower E_L, the higher density of kink atoms at a fixed E_U. In another word, surface structure of Pt nanocrystals is determined by reconstruction of oxygen adsorption/desorption through place-

dx.doi.org/10.1021/ja410583b | J. Am. Chem. Soc. 2013, 135, 18754–18757

exchange, oxidative etching at the E_U, and the growth rate at the E_L.

In conclusion, we have synthesized successfully convex HOH Pt nanocrystals enclosed by 48 {15 5 3} facets for the first time. We further demonstrated that shape evolution of Pt nanocrystals from THH of {*hk*0} facets to HOH of {*hkl*} facets, and finally to TPH of {*hkk*} facets by increasing either the E_U or E_L of the SWP. This shape evolution via gradually changing Miller indices is greatly different from that observed on low-index faceted nanocrystals via truncated forms. The shape evolution of Pt nanocrystals from THH to TPH via HOH or vice versa is accompanied by the decrease of low-coordinated kink atoms, which may be correlated with the competition between preferentially oxidative etching of kink atoms at the E_U and redeposition of Pt atoms at the E_L. The as-prepared Pt micro/nanocrystals with controllable high-index facets could serve as a promising model for studying single particle behaviors, although they are not suitable for practical catalytic applications because of the large particle size. This study provides a new insight into shape-controlled synthesis of Pt nanocrystals with high-index facets and their formation mechanism.

■ ASSOCIATED CONTENT

Supporting Information

Experimental details, detailed SEM and TEM characterization of Pt nanocrystals in Figure 4. This material is available free of charge via the Internet at http://pubs.acs.org.

■ AUTHOR INFORMATION

Corresponding Author

tnsd@xmu.edu.cn; sgsun@xmu.edu.cn

Notes

The authors declare no competing financial interest.

■ ACKNOWLEDGMENTS

This work was supported by grants from Major State Basic Research Development Program of China (2012CB215500), NSFC (21222310, 20933004, 21073152, 21361140374, and 21321062), and Foundation for the Author of National Excellent Doctoral Dissertation of China (201126).

■ REFERENCES

(1) Noorduin, W. L.; Grinthal, A.; Mahadevan, L.; Aizenberg, J. *Science* **2013**, *340*, 832−837.

(2) (a) Xia, Y. N.; Xiong, Y. J.; Lim, B.; Skrabalak, S. E. *Angew. Chem., Int. Ed.* **2009**, *48*, 60−103. (b) Burda, C.; Chen, X. B.; Narayanan, R.; El-Sayed, M. A. *Chem. Rev.* **2005**, *105*, 1025−1102.

(3) (a) Zhou, Z. Y.; Tian, N.; Huang, Z. Z.; Chen, D. J.; Sun, S. G. *Faraday Discuss.* **2008**, *140*, 81−92. (b) Xiong, Y. J.; Wiley, B.; Xia, Y. N. *Angew. Chem., Int. Ed.* **2007**, *46*, 7157−7159. (c) Tian, N.; Zhou, Z. Y.; Sun, S. G. *J. Phys. Chem. C* **2008**, *112*, 19801−19817.

(4) (a) Tao, A. R.; Habas, S.; Yang, P. D. *Small* **2008**, *4*, 310−325. (b) Niu, W. X.; Xu, G. B. *Nano Today* **2011**, *6*, 265−285.

(5) Yin, Y. D.; Alivisatos, A. P. *Nature* **2005**, *437*, 664−670.

(6) (a) Quan, Z. W.; Wang, Y. X.; Fang, J. Y. *Acc. Chem. Res.* **2013**, *46*, 191−202. (b) Jiang, Z. Y.; Kuang, Q.; Xie, Z. X.; Zheng, L. S. *Adv. Funct. Mater.* **2010**, *20*, 3634−3645. (c) Zhou, Z. Y.; Tian, N.; Li, J. T.; Broadwell, I.; Sun, S. G. *Chem. Soc. Rev.* **2011**, *40*, 4167−4185. (d) Niu, Z. Q.; Wang, D. S.; Yu, R.; Peng, Q.; Li, Y. D. *Chem. Sci.* **2012**, *3*, 1925−1929.

(7) Tian, N.; Zhou, Z. Y.; Sun, S. G.; Ding, Y.; Wang, Z. L. *Science* **2007**, *316*, 732−735.

(8) (a) Ming, T.; Feng, W.; Tang, Q.; Wang, F.; Sun, L. D.; Wang, J. F.; Yan, C. H. *J. Am. Chem. Soc.* **2009**, *131*, 16350−16351. (b) Zhang, J. A.; Langille, M. R.; Personick, M. L.; Zhang, K.; Li, S. Y.; Mirkin, C. A. *J. Am. Chem. Soc.* **2010**, *132*, 14012−14014. (c) Tian, N.; Zhou, Z. Y.; Yu, N. F.; Wang, L. Y.; Sun, S. G. *J. Am. Chem. Soc.* **2010**, *132*, 7580−7581. (d) Yu, T.; Kim, D. Y.; Zhang, H.; Xia, Y. N. *Angew. Chem., Int. Ed.* **2011**, *50*, 2773−2777.

(9) Li, Y. Y.; Jiang, Y. X.; Chen, M. H.; Liao, H. G.; Huang, R.; Zhou, Z. Y.; Tian, N.; Chen, S. P.; Sun, S. G. *Chem. Commun.* **2012**, *48*, 9531−9533.

(10) (a) Ma, Y. Y.; Kuang, Q.; Jiang, Z. Y.; Xie, Z. X.; Huang, R. B.; Zheng, L. S. *Angew. Chem., Int. Ed.* **2008**, *47*, 8901−8904. (b) Yu, Y.; Zhang, Q. B.; Lu, X. M.; Lee, J. Y. *J. Phys. Chem. C* **2010**, *114*, 11119−11126.

(11) (a) Zhang, L.; Zhang, J. W.; Kuang, Q.; Xie, S. F.; Jiang, Z. Y.; Xie, Z. X.; Zheng, L. S. *J. Am. Chem. Soc.* **2011**, *133*, 17114−17117. (b) Lee, Y. W.; D., K.; Hong, J. W.; Kang, S. W.; Lee, S. B.; Han, S. W. *Small* **2013**, *9*, 660−665. (c) Yu, Y.; Zhang, Q. B.; Liu, B.; Lee, J. Y. *J. Am. Chem. Soc.* **2010**, *132*, 18258−18265. (d) Hong, J. W.; Lee, S. U.; Lee, Y. W.; Han, S. W. *J. Am. Chem. Soc.* **2012**, *134*, 4565−4568.

(12) (a) Horvath, J. D.; Koritnik, A.; Kamakoti, P.; Sholl, D. S.; Gellman, A. J. *J. Am. Chem. Soc.* **2004**, *126*, 14988−14994. (b) Baber, A. E.; Gellman, A. J.; Sholl, D. S.; Sykes, E. C. H. *J. Phys. Chem. C* **2008**, *112*, 11086−11089. (c) Attard, G. A. *J. Phys. Chem. B* **2001**, *105*, 3158−3167.

(13) (a) Sun, Y. G.; Xia, Y. N. *Science* **2002**, *298*, 2176−2179. (b) Niu, W. X.; Zhang, L.; Xu, G. B. *ACS Nano* **2010**, *4*, 1987−1996. (c) Liu, M. C.; Zheng, Y. Q.; Zhang, L.; Guo, L. J.; Xia, Y. N. *J. Am. Chem. Soc.* **2013**, *135*, 11752−11755. (d) Song, H.; Kim, F.; Connor, S.; Somorjai, G. A.; Yang, P. *J. Phys. Chem. B* **2004**, *109*, 188−193.

(14) Tran, T. T.; Lu, X. M. *J. Phys. Chem. C* **2011**, *115*, 3638−3645.

(15) (a) Inukai, J.; Tryk, D. A.; Abe, T.; Wakisaka, M.; Uchida, H.; Watanabe, M. *J. Am. Chem. Soc.* **2013**, *135*, 1476−1490. (b) Komanicky, V.; Chang, K. C.; Menzel, A.; Markovic, N. M.; You, H.; Wang, X.; Myers, D. *J. Electrochem. Soc.* **2006**, *153*, B446−B451.